Supplemental material for
Finding the cell center by a balance of dynein and myosin pulling and microtubule pushing: a computational study

Jie Zhu*, Anton Burakov†, Vladimir Rodionov‡, Alex Mogilner*,§

*** Department of Neurobiology, Physiology and Behavior and Department of Mathematics, University of California, Davis, CA 95616, USA**

† A. N. Belozersky Institute of Physico-Chemical Biology, Moscow State University, Moscow 119899, Russia

‡ Department of Cell Biology and Center for Cell Analysis and Modeling, University of Connecticut Health Center , Farmington, CT 06032, USA

§ **Corresponding author. E-mail: mogilner@math.ucdavis.edu**

Distribution of microtubule plus-ends

Microtubules (MTs) in interphase cells grow radially from the centrosome (CS), with plus-ends facing outwards and minus-ends anchored in the CS (see Figure 2A). MTs display dynamic instability, during which they in turn grow steadily with speed v_1 and shorten with speed v_2 (see Figure S1). The MTs switch from the growing to the shortening state with the catastrophe rate k_1, and from the shortening to the growing state with the rescue rate k_2. The dynamic instability model we use follows closely the two-state dynamic instability model [1]. We define the densities of the MT plus-ends in the growing and shortening states to be ρ_1 and ρ_2, respectively. The steady-state distribution of the densities ρ_1 and ρ_2 in two-dimensional (2D) space satisfy the conservation equations:

$$\frac{\partial \rho_1}{\partial t} = -\frac{v_1}{r}\frac{\partial}{\partial r}(r\rho_1) - k_1\rho_1 + k_2\rho_2 = 0, \tag{S1}$$

$$\frac{\partial \rho_2}{\partial t} = \quad \frac{v_2}{r}\frac{\partial}{\partial r}(r\rho_2) + k_1\rho_1 - k_2\rho_2 = 0, \tag{S2}$$

where r is the distance from the CS. At the steady state, the outward flux of ρ_1 and the inward flux of ρ_2 should be balanced everywhere, which gives

$$v_1\rho_1 = v_2\rho_2. \tag{S3}$$

At CS ($r = 0$), we assume that new MTs are nucleated at a constant rate k_0 from the CS, and that new MTs are always in the growing state. Then, the nucleation rate of growing MTs should balance the extinction rate of shortening MTs. At the steady state, k_0 should be balanced by the flux of ρ_2 into a small circular area A around the CS with radius $r \to 0$. Let $\vec{v}_2 = -v_2\hat{e}_r$ be the velocity vector of the shortening MTs with $\hat{e}_r$ being the unit radial vector, then the flux balance gives

$$k_0 = -\int_A \nabla\cdot(\vec{v}_2\rho_2)\,\mathrm{d}A = \int_{\partial A} v_2\rho_2\,\mathrm{d}l = 2\pi r v_2\rho_2, \tag{S4}$$

where ∂A is the boundary of the area A, l is the length along ∂A, and the second equality is obtained from Gauss's law. This argument results in the following equation:

$$\rho_2 = \frac{k_0}{2\pi v_2 r} \qquad \text{if } r \to 0. \tag{S5}$$

From Eqs. S1-S5, the steady-state solutions can be found as

$$\rho_1 = \frac{k_0}{2\pi v_1 r}e^{-r/L}, \tag{S6}$$

$$\rho_2 = \frac{k_0}{2\pi v_2 r}e^{-r/L}, \tag{S7}$$

where $L = v_1 v_2/(k_1 v_2 - k_2 v_1)$ is the length scale for MT dynamic instability. Equations S6 and S7 describe MTs in an infinite 2D space. Since the distribution of MTs in a cell is limited by the cell membrane, we assume that MTs in the growing state immediately switch to the shortening state when they reach the cell boundary. With this assumption, the flux balance still holds. Therefore, the expressions for ρ_1 and ρ_2 inside the cell are not affected by the existence of the cell boundary.

The concentration of all MT plus-ends in the cell is the sum of ρ_1 and ρ_2:

$$\rho = \rho_1 + \rho_2 = \frac{k_0}{2\pi v r} e^{-r/L}, \tag{S8}$$

where $v = v_1 v_2/(v_1 + v_2)$. The values of v_1, v_2, k_1 and k_2 are taken from [2] and are given in Table S1. From the same source, we can glean that the cell radius to be $R \approx 20$ μm. Since the total number of MTs in a cell can be calculated as

$$N = 2\pi \int_0^R \rho\, r\, \mathrm{d}r = \frac{k_0 L}{v}\big(1 - e^{-R/L}\big), \tag{S9}$$

we take $k_0 = 100$ min^{-1}, which corresponds to $N \approx 300$. In the continuous deterministic model, we ignore the stochastic effects of the MTs and treat the distribution of the plus-ends of MTs as smooth functions of r as shown above.

Force on the centrosome

In a flat disc-like cell with radius R, we assume that the distance between the CS C and the cell's center O is x (see Figure 2A). A microtubule CP with length r is growing toward the cell periphery B. The angle between the MT and the x-axis is θ. We define $f_x(r, \theta)$ to be the x-component of force on the CS generated by an individual MT with length r and orientation θ. Because of symmetry, the total force on the CS is simply the integral of ρf_x over the entire area of the cell:

$$F_{\mathrm{tot}} = 2\int_0^{\pi} \mathrm{d}\theta \int_0^{r_{\mathrm{m}}} \rho f_x r\, \mathrm{d}r = \frac{k_0}{\pi v} \int_0^{\pi} \mathrm{d}\theta \int_0^{r_{\mathrm{m}}} f_x\, e^{-r/L} \mathrm{d}r, \tag{S10}$$

where r_{m} is the distance from C to the cell periphery at angle θ:

$$r_{\mathrm{m}}(\theta) = \mathrm{CB} = \sqrt{R^2 - x^2 \sin^2\theta} - x\cos\theta. \tag{S11}$$

We consider three possible interaction mechanisms: 1) MTs can be pulled away from the CS by dyneins in the cortex, with force being proportional to MT lengths; 2) MTs can be dragged toward the center of the cell by the actomyosin-driven inward flow of the actin network; and 3) MT growing plus-ends can bump into obstacles in the cortex and push back on the CS. Equation S10 can be expressed as

$$F_{\mathrm{tot}} = F_{\mathrm{dyn}} + F_{\mathrm{act}} + F_{\mathrm{push}}, \tag{S12}$$

where F_{dyn}, F_{act} and F_{push} are the total forces from dynein, actin-flow drag and MTs' pushing, respectively.

Mechanism 1: MTs are pulled by the cortex dyneins

Since dyneins in the cell cortex pull the MT along its length in the outward direction, the pulling force f_{dyn} on each MT is proportional to r:

$$f_{\mathrm{dyn}} = ar, \tag{S13}$$

where a is a constant (dynein force per MT unit length). The force component along the x-direction is

$$f_x = f_{\mathrm{dyn}} \cos\theta. \tag{S14}$$

Then, Eq. S10 gives

$$F_{\rm dyn} = -\frac{aL^2k_0}{\pi v}\int_0^{\pi}(1+u)e^{-u}\cos\theta\,\mathrm{d}\theta, \tag{S15}$$

where $u = r_{\rm m}/L$. Eq. S15 can be solved numerically. Figure 3A shows the $F_{\rm dyn}$-x with $F_{\rm dyn}$ being normalized by the factor aL, which is the characteristic dynein force applied to a MT of length L. For positive x, $F_{\rm dyn}$ is always negative, and the magnitude of $F_{\rm dyn}$ increases with x. Therefore, the CS is always pushed back toward the cell center, so dynein stabilizes the centering of the CS.

Mechanism 2: MTs are dragged by the inward flow

The inward flow of the actin network caused by the actin-myosin contraction produces drag forces on the MTs. The drag force on each segment of a MT is proportional to the velocity of the flow, and is pointing toward the cell's center O. We assume that the actin network's flow speed at a displacement $\vec{d}$ from point O is proportional to $-\vec{d}$:

$$\vec{v}_{\rm flow}(d) \propto -\vec{d}. \tag{S16}$$

This assumption is in qualitative agreement with experimental observations; it can also be justified with the following argument. In a disc-shaped shell of actin network that is centered at O with radius r and area $A = \pi r^2$, the shrinking rate of the network due to actomyosin contraction is proportional to the amount of myosin inside this region, which is proportional to A. Therefore, the shrinking rate of this region is

$$-\frac{\mathrm{d}A}{\mathrm{d}t} \propto A \propto r^2. \tag{S17}$$

The velocity of the inward flow at distance r from the cell center is simply the shrinking rate of the network radius at r:

$$v_{\rm flow} = \left|\frac{\mathrm{d}r}{\mathrm{d}t}\right| = \left|\frac{\mathrm{d}r}{\mathrm{d}A}\frac{\mathrm{d}A}{\mathrm{d}t}\right| \propto r. \tag{S18}$$

For a segment of MT that is at a distance s from the CS C (see Figure 2A), its displacement from point O is

$$\vec{d}(s) = \vec{x} + s\hat{n}, \tag{S19}$$

where $\hat{n}$ is the direction of MT growth. We assume that the force density on the segment is proportional to $\vec{v}_{\rm flow}$. From Eq. S16, the total force on the MT is the integral of drag forces on the MT:

$$\vec{f}_{\rm act} = -b\int_0^r \vec{d}\,\mathrm{d}s = -b\left(r\vec{x} + \frac{r^2}{2}\hat{n}\right), \tag{S20}$$

where b is a constant (drag force per unit area). Then, the value of the force component f_x is

$$f_x = \vec{f}_{\rm act}\cdot\hat{e}_x = -b\left(rx + \frac{r^2}{2}\cos\theta\right), \tag{S21}$$

where $\hat{e}_x$ is the unit vector in the x-direction. Thus, the total force on the CS can be obtained from Eq. S10 as

$$F_{\rm act} = -\frac{bL^2xk_0}{v} + \frac{bL^3k_0}{\pi v}\int_0^{\pi}\left[\left(1+u+\frac{u^2}{2}\right)\cos\theta + \frac{x}{L}(1+u)\right]e^{-u}\mathrm{d}\theta. \tag{S22}$$

Figure 3A shows the $F_{\rm act}$-x relation with $F_{\rm act}$ being normalized by bL^2, which is the characteristic drag force on a MT of length L at a distance L from the cell center. Similar to mechanism 1, for positive values of x, $F_{\rm act}$ is always negative. Thus, the CS is always pushed by myosin-driven flow toward the center of the cell. This mechanism also stabilizes the CS centering.

Mechanism 3: growing MTs plus-ends push on structures that are uniformly scattered in the cortex

Growing MTs can bump into obstacles in the cortex. We assume that the obstacles are evenly distributed in the cortex, and that the average force on each individual growing MT is proportional to the frequency of collisions. Since v_1 is a constant, the frequency of collisions should be the same for all the growing MTs, so the average force on each growing MT should be the same. We define that average force with which each growing MT pushes back on the CS as f_{push}. Then the x-component of the force (see Figure 2A) is

$$f_x = -f_{\text{push}} \cos\theta. \tag{S23}$$

By replacing ρ with ρ_1 in Eq. S10, the total force on the CS can be obtained as

$$F_{\text{push}} = \frac{f_{\text{push}} L k_0}{\pi v_1} \int_0^\pi e^{-u} \cos\theta \, \mathrm{d}\theta. \tag{S24}$$

The normalized F_{push}-x relation is shown in Figure 3A. For positive x, F_{push} is always positive, and the magnitude of F_{push} increases as x increases. Therefore, this force would push the CS away from the cell center and de-stabilize the centering.

Effects of local application of nocodazole

Figures 2E-F, 3C show the schematics of a cell with a partially cut MT aster by the local application of nocodazole. We assume that the cut is made perpendicular to the x-axis at $x = -x_{\text{c}}$ (see Figure S2). Let D be one of the intersections between the cutting line and the cell periphery, the angle between line DC and the x-axis is

$$\theta_{\text{c}} = \pi - \tan^{-1}\left(\frac{h}{x + x_{\text{c}}}\right), \tag{S25}$$

where $h = \sqrt{R^2 - x_{\text{c}}^2}$ is the half-length of the cutting line. We define $r'_{\text{m}}(\theta)$ to be the maximum length of MTs with angle θ after the cut is made. It is easy to find that r'_{m} satisfies

$$r'_{\text{m}}(\theta) = \begin{cases} r_{\text{m}}(\theta) & \text{if } 0 \le \theta \le \theta_{\text{c}}, \\ -(x + x_{\text{c}})/\cos\theta & \text{if } \theta_{\text{c}} < \theta \le \pi. \end{cases} \tag{S26}$$

We assume that when the growing MTs reach the cutting line, they immediately convert to the shortening state. Similar to the effect of the cell boundary, the existence of the cutting line does not change the distributions ρ_1 and ρ_2 inside the region that is unaffected by nocodazole. Therefore, the forces on the CS in mechanisms 1–3 can still be obtained from Eqs. S15, S22 and S24 by replacing u with $u' = r'_{\text{m}}/L$:

$$F'_{\text{dyn}} = -\frac{aL^2 k_0}{\pi v} \int_0^\pi (1 + u') e^{-u'} \cos\theta \, \mathrm{d}\theta, \tag{S27}$$

$$F'_{\text{act}} = -\frac{bL^2 x k_0}{v} + \frac{bL^3 k_0}{\pi v} \int_0^\pi \left[\left(1 + u' + \frac{u'^2}{2}\right)\cos\theta + \frac{x}{L}(1 + u')\right] e^{-u'} \mathrm{d}\theta, \tag{S28}$$

$$F'_{\text{push}} = \frac{f_{\text{push}} L k_0}{\pi v_1} \int_0^\pi e^{-u'} \cos\theta \, \mathrm{d}\theta. \tag{S29}$$

Forces' dependencies on the distance computed with these integrals are shown in Figure S3, A–C. As x_{c} decreases, more MTs are cut, force F'_{dyn} shifts toward the positive direction because the pulling force along the negative x-direction is reduced by the cutting of respective MTs. The equilibrium position of the CS also shifts toward the positive x-direction, which indicates that the CS tends to move away from the nocodazole source. F'_{act} shifts to the negative x-direction for small x, but to the positive direction at large x. Therefore, previously centered CS tends to move toward the nocodazole source. F'_{push} shifts toward the negative x-direction, because the opposing forces on MTs in that direction decreases. The CS tends to move toward the nocodazole source.

The overall effect on the CS's positioning should be the sum of all three mechanisms. Although the values of the force constants a, b and f_{push} are unknown, their relative magnitudes are constrained by the experimental observations as discussed in the main text.

Constraints on the parameters from the experimental results

For an initially centered CS in a disc-like cell that is unaffected by nocodazole, forces $F_{\rm dyn}$, $F_{\rm act}$ and $F_{\rm push}$ are always zero at $x = 0$. Therefore, the CS's direction of motion at $x = 0$ is determined by the sign of the x-derivative of the total force. For an initially centered CS in a nocodazole-applied cell, forces $F'_{\rm dyn}$, $F'_{\rm act}$ and $F'_{\rm push}$ are non-zero. Thus the CS's direction of motion is determined by the sign of the total force at $x = 0$.

Cell unaffected by nocodazole. In the control, the CS is stable at the cell center. In our model, this can be formulated as

$$\left(\frac{\partial F_{\rm dyn}}{\partial x} + \frac{\partial F_{\rm act}}{\partial x} + \frac{\partial F_{\rm push}}{\partial x}\right)\Big|_{x=0} < 0. \tag{S30}$$

Observation 1. When dynein is inhibited, the CS moves away from the center to the cell periphery. In this case, only mechanisms 2 and 3 contribute to the force. The following should hold:

$$\begin{aligned} \left(\frac{\partial F_{\rm act}}{\partial x} + \frac{\partial F_{\rm push}}{\partial x}\right)\Big|_{x=0} &> 0, \\ (F_{\rm act} + F_{\rm push})|_{0<x\leq R} &> 0. \end{aligned} \tag{S31}$$

Observation 2. When myosin is inhibited, the CS stays at the center. In this case, only mechanisms 1 and 3 have contributions:

$$\left(\frac{\partial F_{\rm dyn}}{\partial x} + \frac{\partial F_{\rm push}}{\partial x}\right)\Big|_{x=0} < 0. \tag{S32}$$

Observation 3. When both dynein and myosin are inhibited, the CS moves away from the center. In our model, it can be formulated as

$$\frac{\partial F_{\rm push}}{\partial x}\Big|_{x=0} > 0. \tag{S33}$$

Observation 4. When dynein is inhibited and the dynamics of MTs is inhibited by taxol, the CS stays at the center. This can be expressed as

$$\frac{\partial F_{\rm act}}{\partial x}\Big|_{x=0} < 0. \tag{S34}$$

Observation 5. When nocodazole is applied locally, the CS moves toward the nocodazole source. This indicates

$$(F'_{\rm dyn} + F'_{\rm act} + F'_{\rm push})|_{x=0} < 0. \tag{S35}$$

Observation 6. If nocodazole is applied locally to a myosin-inhibited cell, the CS moves away from the nocodazole source. In our model, this shows

$$(F'_{\rm dyn} + F'_{\rm push})|_{x=0} > 0. \tag{S36}$$

Observation 7. In addition to observation 6, when dynein is weakened by the inhibition of Cdc42, the CS oscillates near the cell center. This can be written as

$$(\epsilon F'_{\rm dyn} + F'_{\rm push})|_{x=0} = 0, \tag{S37}$$

where $0 < \epsilon < 1$ is a factor indicating the weakening of dynein action.

Among the above equations, Eqs. S33 and S34 are always satisfied in our model, and Eq. S37 is similar to Eq. S36. The suitable range of $aL/f_{\rm push}$ and $bL^2/f_{\rm push}$ for each of the rest of the equations are shown in Figure 6B. The range of parameter values that can satisfy all the experimental observation is the intersection of all those regions. We find that the final range of parameters is simply determined by Eqs. S31, S35 and S36.

Figure 6C shows the ranges of $aL/f_{\rm push}$ and $bL^2/f_{\rm push}$ that will satisfy all the experimental observations for various cell shapes and sizes. We find that for cells with a similar shape, the suitable range of parameters decreases as the size of the cell increases. For a circular cell, when R increases from 20 μm to 40 μm, both the maximum and the minimum values of $aL/f_{\rm push}$ decrease by a factor of 2, while the maximum value of $bL^2/f_{\rm push}$ decreases roughly by a factor of 4. To understand this result, we consider an extreme case where $L \to \infty$ and find $F_{\rm dyn} \propto aR$, $F_{\rm act} \propto bR^2$ and $F_{\rm push} \propto f_{\rm push}$. Indeed, for the case of $L \to \infty$, the term $e^{-r/L}$ disappears from Eq. S10:

$$F_{\rm tot} = \frac{k_0}{\pi v}\int_0^{\pi} \mathrm{d}\theta \int_0^{r_{\rm m}} f_x \mathrm{d}r. \tag{S38}$$

For mechanism 1, Eq. S38 becomes

$$F_{\rm dyn} = \frac{ak_0}{2\pi v}\int_0^{\pi} r_{\rm m}^2 \cos\theta \,\mathrm{d}\theta \approx -\frac{aRk_0}{2v}x. \tag{S39}$$

The last term is obtained by approximating $r_{\rm m}^2 \approx R^2 - 2xR\cos\theta$ for $|x| \ll R$. For mechanism 2, without expanding $r_{\rm m}$ near $x = 0$, the following relations can be found by keeping only the even terms regarding to $\theta = \pi/2$:

$$\int_0^{\pi} r_{\rm m}^3 \cos\theta \,\mathrm{d}\theta = -\frac{3\pi}{2}R^2 x, \tag{S40}$$

$$\int_0^{\pi} r_{\rm m}^2 \,\mathrm{d}\theta = \pi R^2. \tag{S41}$$

Eq. S38 then gives

$$F_{\rm act} = -\frac{bk_0}{\pi v}\int_0^{\pi}\left(\frac{1}{6}r_{\rm m}^3\cos\theta + \frac{1}{2}xr_{\rm m}^2\right)\mathrm{d}\theta = -\frac{bR^2k_0}{4v}x. \tag{S42}$$

For mechanism 3, by keeping the even terms with respect to $\theta = \pi/2$, Eq. S38 becomes

$$F_{\rm push} = -\frac{f_{\rm push}k_0}{\pi v_1}\int_0^{\pi} r_{\rm m}\cos\theta \,\mathrm{d}\theta = \frac{f_{\rm push}k_0}{2v_1}x. \tag{S43}$$

This indicates that to keep a certain balance between $F_{\rm dyn}$, $F_{\rm act}$ and $F_{\rm push}$, factors a and b should satisfy $a \propto 1/R$ and $b \propto 1/R^2$. We find numerically that this relation still roughly holds if L is greater than or comparable to R.

Figure 6C also shows that the suitable range of $aL/f_{\rm push}$ and $bL^2/f_{\rm push}$ can be affected by the shape of the cells. Given the same cell area, an elliptical cell has a greater range of suitable parameter values than a circular cell has. This is mainly because of the increased maximum value of $bL^2/f_{\rm push}$, which is determined by the dynein-inhibition experiment. In this experiment, if the CS moves away from the center along the short-axis of the cell, the effective size of the cell becomes smaller than R. From the analysis above, the cell will allow for a higher maximum value of $bL^2/f_{\rm push}$. The shape of the cells affects $aL/f_{\rm push}$ in a similar way. The minimum value of $aL/f_{\rm push}$ is determined by the nocodazole-application experiment on myosin-inhibited cells. If the nocodazole is applied at one of the pointed ends of the cell, the motion of the CS should be along the long-axis of the cell. Then, the effective size of the cell becomes greater than R, which results in a decreased minimum value of $aL/f_{\rm push}$ as shown in Figure 6C. On the other hand, if the nocodazole is applied at one of the flat sides of the cell, the motion of the CS should be along the short-axis of the cell. If the CS still moves away from the nocodazole source, the effective size of the cell would become smaller than R and would lead to an increased minimum value of $aL/f_{\rm push}$.

We notice that in our previous study [2], MTs in some cells tend to form parallel patterns along the cell's long-axis. To evaluate the influence of the orientational anisotropicity in the distribution of MTs,

we study a one-dimensional (1D) model as an extreme case for all MTs being perfectly aligned. In 1D, Eqs. S1 and S2 become

$$\frac{\partial \rho_1}{\partial t} = -v_1 \frac{\partial \rho_1}{\partial r} - k_1 \rho_1 + k_2 \rho_2 = 0, \tag{S44}$$

$$\frac{\partial \rho_2}{\partial t} = \quad v_2 \frac{\partial \rho_2}{\partial r} + k_1 \rho_1 - k_2 \rho_2 = 0. \tag{S45}$$

Considering the flux balance conditions of $v_1\rho_1 = v_2\rho_2$ for any r and $k_0 = v_2\rho_2$ for $r \to 0$, the solutions of the above equations are

$$\rho_1 = \frac{k_0}{v_1} e^{-r/L}, \tag{S46}$$

$$\rho_2 = \frac{k_0}{v_2} e^{-r/L}. \tag{S47}$$

The total density of plus-ends is

$$\rho = \rho_1 + \rho_2 = \frac{k_0}{v} e^{-r/L}. \tag{S48}$$

Assuming the CS is at x and the half-length of the cell is R, the distances from the CS to the left and right cell boundaries are $R + x$ and $R - x$, respectively. For mechanism 1, the total force on the CS is

$$\begin{aligned} F_{\text{dyn}} &= -\int_0^{R+x} \rho\, r \,\mathrm{d}r + \int_0^{R-x} \rho\, r \,\mathrm{d}r = -\frac{ak_0}{v} \int_{R-x}^{R+x} r\, e^{-r/L} \,\mathrm{d}r \\ &= -\frac{aL^2 k_0}{v} \left[(1+u_1)e^{-u_1} - (1+u_2)e^{-u2}\right], \end{aligned} \tag{S49}$$

where $u_1 = (R-x)/L$ and $u_2 = (R+x)/L$. For mechanism 2, similar to the calculations in Eq. S20, the forces on a left-growing and right-growing MT are $f_L = -b(xr - r^2/2)$ and $f_R = -b(xr + r^2/2)$, respectively. Then, the total force on the CS is

$$\begin{aligned} F_{\text{act}} &= \int_0^{R+x} \rho f_L \mathrm{d}r + \int_0^{R-x} \rho f_R \mathrm{d}r \\ &= -\frac{bL^2 x k_0}{v} \left[2 - (1+u_1)e^{-u_1} - (1+u_2)e^{-u2}\right] \\ &\quad + \frac{bL^3 k_0}{v} \left[\left(1 + u_1 + \frac{u_1^2}{2}\right)e^{-u_1} - \left(1 + u_2 + \frac{u_2^2}{2}\right)e^{-u2}\right]. \end{aligned} \tag{S50}$$

For mechanism 3, the total force is simply

$$F_{\text{push}} = \int_0^{R+x} \rho_1 f_{\text{push}} \mathrm{d}r - \int_0^{R-x} \rho_1 f_{\text{push}} \mathrm{d}r = \frac{f_{\text{push}} k_0}{v_1} \int_{R-x}^{R+x} e^{-r/L} \mathrm{d}r = \frac{f_{\text{push}} L k_0}{v_1} \left(e^{-u_1} - e^{-u_2}\right). \tag{S51}$$

When the nocodazole is applied at x_c on the left of the cell center, the cutting line now becomes the left boundary of the MTs. The distance from the CS to the cut is $x_c + x$. By replacing u_2 with $u_3 = (x_c + x)/L$ in Eqs. S49–S51, one obtains the total forces on the CS with the application of nocodazole. For $L \to \infty$, Eqs. S49–S51 become

$$F_{\text{dyn}} = -\frac{2aRk_0}{v} x, \tag{S52}$$

$$F_{\text{act}} = -\frac{2bk_0}{3v} x^3, \tag{S53}$$

$$F_{\text{push}} = \frac{2f_{\text{push}} k_0}{v_1} x. \tag{S54}$$

The suitable parameter values for a 1D cell are also shown in Figure 6C. The most noticeable difference is that the maximum value of $bL^2/f_{\rm push}$ is higher than that of circular or elliptical cells. The reason is that the centering effect from the myosin contraction flow is much weaker in 1D. In a limiting case of $L \to \infty$, we find $\mathrm{d}F_{\rm act}/\mathrm{d}x \propto x^2 \approx 0$ near $x = 0$. Therefore, to keep a certain balance between $F_{\rm act}$ and $F_{\rm push}$, a higher maximum value of b is allowed.

Figure 6C allows us to choose suitable values of $aL/f_{\rm push}$ and $bL^2/f_{\rm push}$, and then evaluate the motion of the CS under various conditions. For a cell with $R = 20$ μm, we choose $aL/f_{\rm push} = 3$ and $bL^2/f_{\rm push} = 8$. The total forces on the CS under various conditions are shown in Figure 3, B and F. Once the total force on the CS is found, the CS's motion can be obtained as

$$\frac{\mathrm{d}x}{\mathrm{d}t} = \mu F_{\rm tot}, \tag{S55}$$

where μ is the mobility of the CS. To estimate the value of μ, we consider the following reasoning. We assume that the CS's mobility is determined by the interactions between the MT aster and the actin networks. In mechanism 2, the dragging force on a MT segment of length s can be written as $f_{\rm s} = \zeta_{\rm s} v_{\rm flow}$, where $\zeta_{\rm s}$ is the friction constant of the segment. We take $v_{\rm flow} = \alpha d$ and $\zeta_{\rm s} = \beta s$, where α and β are constants. Comparing to Eq. S20, we have $\alpha\beta = b$. For the CS, we estimate its friction coefficient to be $\zeta = \beta l_{\rm tot}$, where $l_{\rm tot}$ is the total length of all the MTs in the aster:

$$l_{\rm tot} \approx 2\pi \int_0^R \rho\, r^2 \mathrm{d}r = \frac{k_0 L^2}{v}\left[1 - \left(1 + \frac{R}{L}\right)e^{-R/L}\right]. \tag{S56}$$

The CS's mobility can be written as $\mu = 1/\zeta = \alpha/b l_{\rm tot}$. We take $\alpha = 0.1$ min^{-1}, which corresponds to a flow rate of 2 μm/min at a distance of 20 μm from the cell center [3]. For $b = 8 f_{\rm push}/L^2$, $k_0 = 100$ s^{-1} and $L = 60$ μm, we find $l_{\rm tot} \approx 3000$ μm and $\mu f_{\rm push} \approx 0.02$ μm/min. We estimate $f_{\rm push} \sim 0.6$ pN (see main text), then we have $\mu \sim 0.03$ μm/(pN·min).

Stochastic simulations

To check our analytical results, we have also performed stochastic simulations in a 2D space. In the simulations, we assume that new MTs are created at the CS at rate k_0 with zero initial lengths and random growth directions, and that each growing MT elongates at speed v_1 until it switches to the shortening state. We treat the switching events as a Poisson process, in which the occurrence of the switching within time τ follows a Poisson interval distribution $P_1(\tau) = k_1 e^{-k_1\tau}$. The growth duration τ that is associated with each MT is obtained using a random number generator with exponential distribution. Each MT then switches to the shortening state after this particular time. At the shortening state, each MT shortens at velocity v_2 until its length reaches zero. Similar to the calculation of the growth duration, the shortening duration τ that is associated with each MT is obtained from the distribution $P_2(\tau) = k_2 e^{-k_2\tau}$. At the end of the shortening state, if the length of the MT remains positive, the MT switches to the growing state again. In addition to these switching events, the cell periphery and the application of nocodazole prevent further elongation of MTs. In the simulations, this effect is treated by immediately switching the MTs into the shortening state when the MTs reach these regions.

The simulation time step is chosen to be smaller than 1/10 of the inverse of the growth/shortening rate, such that on average each growth/shortening state lasts for at least 10 time steps. At each time step, the force on each MT is calculated from our analytical equations (see Eqs. S10 and S15). The total force on the CS is obtained by summing up forces from all the MTs. The motion of the CS is then determined by Eq. S33 in a vector form in 2D.

Our stochastic simulations agree well with the analytical results. In the stochastic simulations, we also find that in a dynein-inhibited elliptical cell, the CS tends to move away from the cell center along

the short-axis of the cell, which agrees with the experimental observations [2]. This can be explained as follows. The motion of the CS in this experiment is determined only by the force balance between the centering force F_{act} and the de-centering force F_{push}. The magnitude of F_{act} is very sensitive to the size of the cell, because the speed of the myosin contraction flow is assumed to be proportional to the distance from the cell center. Therefore, in an elliptical cell, F_{act} is weaker along the short-axis than along the long-axis. On the other hand, F_{push} is less affected by the geometry of the cell, because most of the growing ends of the MTs are distributed near the CS (see Eq. S6). Thus, the magnitude of F_{push} is roughly independent of the CS's moving direction. The combined effect is that the CS is more likely to move away from the cell center along the short-axis of the cell.

Dynein pulling from the boundary

The experimental observations [2] indicate that dyneins stabilize the centering of the CS. In our model, we treat the force from the dyneins on a MT to be proportional to the length of the MTs. This assumption requires dyneins to be evenly distributed in the cortex. There is another possible dynein-dependent mechanism that can give similar results [4]: pulling from sparsely distributed dyneins at the cell periphery.

If the number of dyneins on the cell periphery is much lower than the number of MTs being in touch with the cell periphery, the pulling force is limited by the availability of dyneins and is therefore independent of the density of MTs. Assuming that N_{dyn} dynein molecules are evenly distributed along the cell periphery, the linear density of the dyneins is $\rho_{\mathrm{dyn}} = N_{\mathrm{dyn}}/2\pi R$. If each dynein exerts a constant pulling force f_1 on a MT (see Figure S4A, the x-component of the force is $f_x = f_1 \cos\theta$. It is easy to find $\cos\theta = (R\cos\varphi - x)/r_{\mathrm{m}}$, where $r_{\mathrm{m}} = \sqrt{R^2 + x^2 - 2Rx\cos\varphi}$. Because of symmetry, the total force from the dyneins on the CS is along the x-direction:

$$F_{\mathrm{dyn}}^{\mathrm{bnd}} = 2\int_0^{\pi} \rho_{\mathrm{dyn}} f_x R \,\mathrm{d}\varphi = \frac{N_{\mathrm{dyn}} f_1}{\pi} \int_0^{\pi} \frac{R\cos\varphi - x}{r_{\mathrm{m}}} \,\mathrm{d}\varphi. \tag{S57}$$

We used Eq. S57 to find the regions of parameter values (Figure S4B) that satisfy all experimental constraints. We found that these constraints can be satisfied only for $0 < x_{\mathrm{c}} < R/4$. This figure indicates that the region of suitable parameters is very sensitive to the value of x_{c}, so this mechanism would not be very robust.

Figures S4C and S4D show the F-x relations for boundary dynein and cortex dynein in nocodazole-affected normal cells, respectively. We focus on the differences near $x = 0$, since the CS was initially close to the cell center in the experiment. We can see that as x_{c} decreases (nocodazole-affected region increases), force from the cortex dyneins at $x = 0$ increases evenly, while the force from boundary dyneins increases rapidly at high x_{c}, but more slowly at low x_{c}. This trend can be seen more clearly in Figure S4E, where the normalized dynein forces at $x = 0$ are shown as functions of x_{c}. At high x_{c} (less cut), force from the boundary dynein is significantly higher than that from the cortex dynein, so the CS is more likely to move in the positive x-direction, which is against the experimental observation. At low x_{c} (more cut), force from the boundary dynein is comparable to that from the cortex dynein, therefore the other two mechanisms are able to counteract this force and pull the CS in the negative x-direction, which agrees with the experiment. Our conclusion is that due to geometric reasons (line versus area), the force from the boundary dyneins is greater than that from the cortex dyneins, especially at high x_{c} values. This would make the CS more likely to move away from the nocodazole source, which disagrees with the observations. Therefore, the boundary dynein pulling mechanism requires far more stringent constraints on the model parameters, which makes it less likely.

Kinesin pushing along the MT lengths

The forces on the CS from kinesins have a similar form as those from dyneins, albeit with an opposite sign and a different prefactor c indicating different kinesin density and strength. The kinesin force on a MT of length r can be written as $f_{\rm kin} = -cr$. Since dynein motors produce the centering forces on the centrosome, kinesin motors produce the de-centering forces. We replace the MT pushing mechanism with this kinesin-pushing mechanism, and scale the dynein and myosin forces with cL. The parameter space satisfying all experimental constraints is shown in Figure S5A. We choose $aL = 1.2cL$ and $bL^2 = 3cL$ (star in Figure S5A) and plotted the F-x relations for the net forces on the CS without (Figure S5B) and with (Figure S5C) nocodazole. These plots show that the kinesin pushing mechanism can have the similar de-centering effect to the MT-pushing action.

Calculations and results for the square and fan-shaped cells

We introduced the anisotropic and isotropic components of the centripetal actin flow field as follows. The isotropic component is given by the formula

$$\vec{v}_{\rm iso} = -\alpha\vec{r}, \tag{S58}$$

while the anisotropic one is defined by

$$\vec{v}_{\rm aniso} = \begin{cases} 0 & \text{if } y \geq 0, \\ \alpha'\left(\dfrac{y^2}{r^2}\right)\vec{r} & \text{if } y < 0, \end{cases} \tag{S59}$$

where α and α' are constants. In the case of the square cell we use just the isotropic flow. For the fan-shaped cell, the net flow is given by (see Figure 7A)

$$\vec{v} = \vec{v}_{\rm iso} + \vec{v}_{\rm aniso} = \begin{cases} -\alpha\vec{r} & \text{if } y \geq 0, \\ -\alpha\left[1 - g\left(\dfrac{y^2}{r^2}\right)\right]\vec{r} & \text{if } y < 0, \end{cases} \tag{S60}$$

where $g = \alpha'/\alpha < 1$ is the reduction factor of the net field at the rear. In the simulations, we choose $g = 0.5$.

The total drag force on a MT is the sum of the forces from the flow. Considering a MT with one end at $\vec{r}_1 = (x_1, y_1)$ and the other at $\vec{r}_2 = (x_2, y_2)$ (see Figure S6), its length is $l = |\vec{r}_2 - \vec{r}_1|$ and direction is $\hat{n} = (n_x, n_y) = (\vec{r}_2 - \vec{r}_1)/l$. The coordinates of any point on the MT can be expressed as $\vec{r} = (x, y) = \vec{r}_1 + s\hat{n}$, where s is the distance between the point and $\vec{r}_1$. The drag force on the MT from field $\vec{v}_{\rm iso}$ is

$$\vec{f}_{\rm iso} = \beta\int_0^l \vec{v}_{\rm iso}{\rm d}s = -b\left(l\vec{r}_1 + \frac{l^2}{2}\hat{n}\right), \tag{S61}$$

where $\beta = b/\alpha$, as defined previously, is the friction constant per MT length. If the MT is completely in the $y \geq 0$ region, the drag force from field $\vec{v}_{\rm aniso}$ is 0. If it is completely in the $y < 0$ region, the drag force from field $\vec{v}_{\rm aniso}$ is

$$\vec{f}_{\rm aniso} = \beta\int_0^l \vec{v}_{\rm aniso}{\rm d}s = b'\int_0^l \left(\frac{y^2}{r^2}\right)\vec{r}{\rm d}s, \tag{S62}$$

where $b' = \alpha'\beta = gb$ and $y = y_1 + sn_y$. The x- and y-components of $\vec{f}_{\rm aniso}$ can be found as

$$f_{{\rm aniso},x} = \frac{b'}{2}\{BC^2 n_x(1 - 4n_y^2) + 2AC^2 n_y(4n_x^2 - 1) + ln_y[ln_x n_y + 2n_x^2 C + 2(n_y^3 x_1 + n_x^3 y_1)]\}, \tag{S63}$$

$$f_{{\rm aniso},y} = \frac{b'}{2}[-2AC^2 n_x(1 - 4n_y^2) + BC^2 n_y(4n_x^2 - 1) + ln_y^2(ln_y + 2y_1 + 4n_x C)], \tag{S64}$$

where A, B and C are given by

$$A = \tan^{-1}\left[\frac{n_x y_1 - n_y x_1}{l + n_x x_1 + n_y y_1}\right], \tag{S65}$$

$$B = \ln[l^2 + 2l(n_x x_1 + n_y y_1) + x_1^2 + y_1^2], \tag{S66}$$

$$C = n_x y_1 - n_y x_1. \tag{S67}$$

If the MT is partly in the $y \geq 0$ region and partly in the $y < 0$ region, the drag force from field $\vec{v}_{\text{aniso}}$ acts only on the part that is in the $y < 0$ region. Then, the total force on the MT is

$$\vec{f} = \vec{f}_{\text{iso}} + \vec{f}_{\text{aniso}}. \tag{S68}$$

If the flow center is not at the origin but at $(x_{\text{flow}}, y_{\text{flow}})$, the drag force can be obtained by simply replacing (x_1, y_1) with $(x_1 - x_{\text{flow}}, y_1 - y_{\text{flow}})$ in the above equations.

Based on the above force calculations, we performed stochastic simulations in the fan-shaped cell. The main results are described in the main text. Interesting additional results include: (i) when dynein is inhibited, the CS shifts to the sharp corner; (ii) when either myosin is inhibited or nocodazole is applied locally, the CS's shift from the centroid of the cell is not dramatic – the CS remains closer to the centroid than to any of the cell edges.

References

1. Dogterom M, Leibler S (1993) Physical aspects of the growth and regulation of microtubule structures. Phys Rev Lett 70: 1347-1350.

2. Burakov A, Nadezhdina E, Slepchenko B, Rodionov V (2003) Centrosome positioning in interphase cells. J Cell Biol 162: 963-969.

3. Yam PT, Wilson CA, Ji L, Hebert B, Barnhart EL, et al. (2007) Actin-myosin network reorganization breaks symmetry at the cell rear to spontaneously initiate polarized cell motility. The Journal of Cell Biology 178: 1207-1221.

4. Vallee RB, Stehman SA (2005) How dynein helps the cell find its center: a servomechanical model. Trends Cell Biol 15: 288-294.

Table and Figures

Table S1. Definition of symbols and parameter values (known values are from Ref. [2]).

Symbol	Definition	Value
v_1	MT's growing velocity	7.5 μm/min
v_2	MT's shortening velocity	16 μm/min
k_1	Switching rate from growing to shortening state	2 min^{-1}
k_2	Switching rate from shortening to growing state	4 min^{-1}
R	Cell radius	20 μm
L	length scale for MT dynamic instability	60 μm
k_0	MT's nucleation rate	100 min^{-1}
ρ_1	Plus-end density of growing MTs	varies
ρ_2	Plus-end density of shortening MTs	varies
ρ	Plus-end density of all MTs	varies
x	Distance between centrosome and cell center	varies
a	Dynein's pulling force per unit length	unknown
b	Actomyosin's drag force per unit area	unknown
f_{push}	Average pushing force per growing MT	unknown

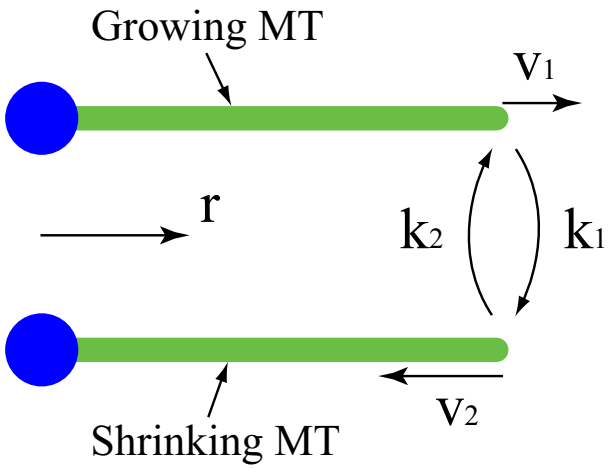

Figure S1. Schematic of the dynamics of MTs (green lines). In the growing state, MTs grow with speed v_1 and can switch to the shortening state with rate k_1. In the shortening state, MTs shorten with speed v_2 and can switch to the growing state with rate k_2. Blue circles represent the centrosome.

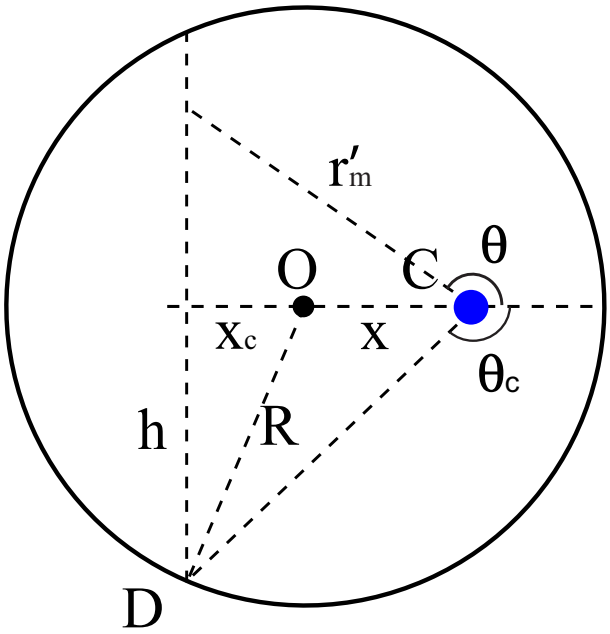

Figure S2. Schematic of a cell with nocodazole applied to the left. Blue dot: centrosome.

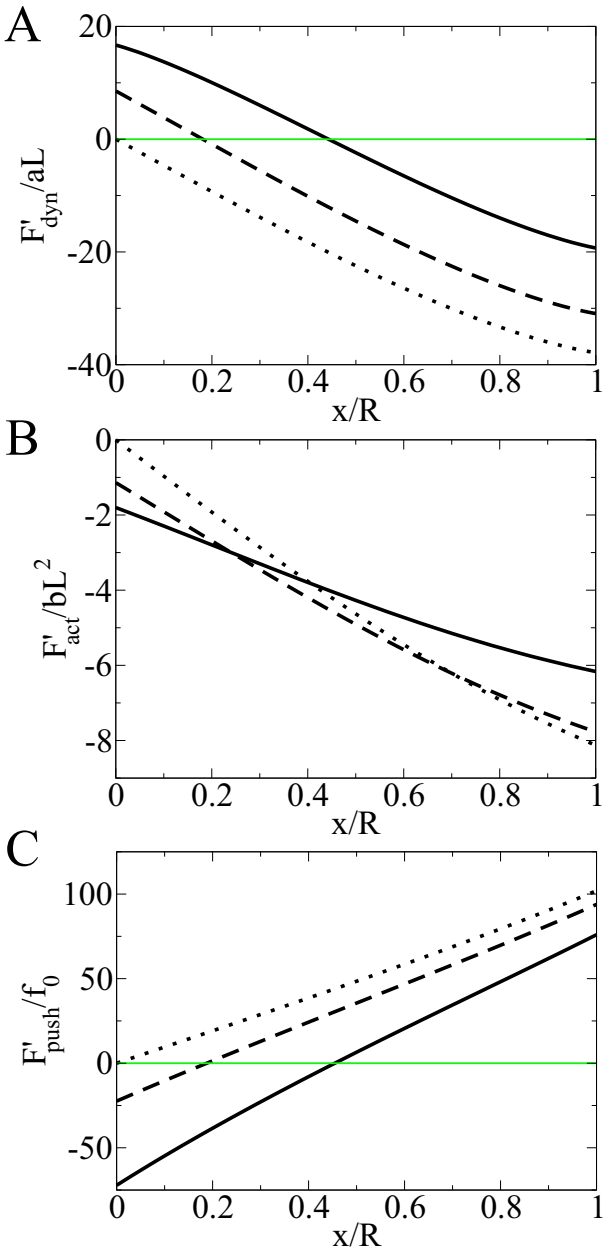

Figure S3. (A-C) Normalized forces on the CS from dynein (A), myosin (B) and pushing (C) mechanisms in the nocodazole-treated cell. The normalization of the forces is the same as those in Figure 3A. The dotted lines, for comparison, correspond to the control cell. The dashed lines correspond to the cell with the nocodazole-affected wedge extending half-way to the center. The solid lines correspond to the nocodazole-affected wedge extending all the way to the cell center.

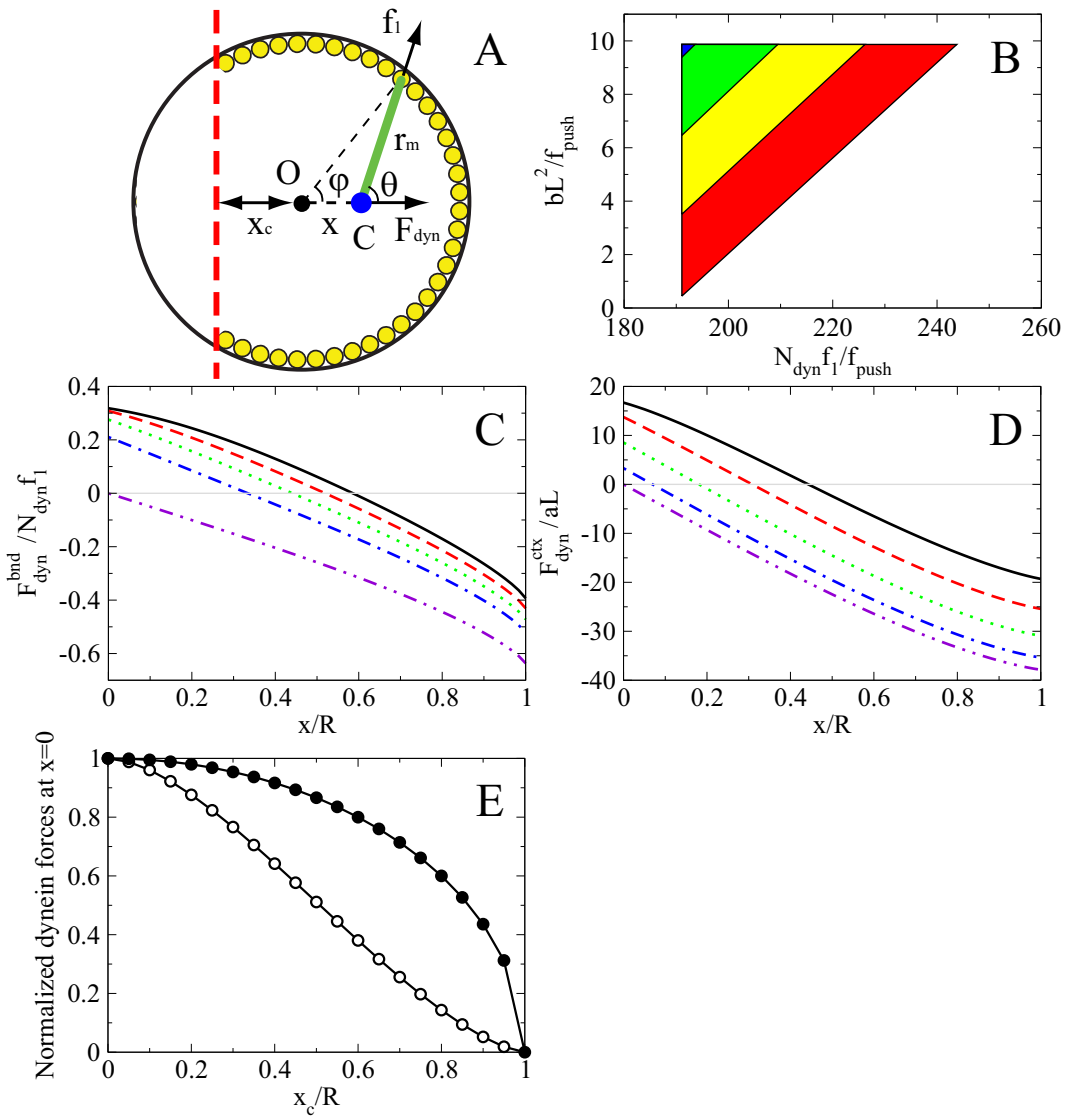

Figure S4. Alternative model with dynein molecules sparsely distributed on the cell periphery instead of across the cortex. (A) Schematic of the force calculation. Each dynein molecule (yellow circles) exerts a pulling force f_1 on the CS (blue circle) through MTs (green line). The net force from all the dyneins on the CS is $F_{\rm dyn}$. The nocodazole affected region is on the left side of the red dashed line at the distance $x_{\rm c}$ from the cell center. (B) The rectangular parameter regions satisfying all experimental constraints for various values of $x_{\rm c}$. Red: $x_{\rm c} = 0.1R$. Yellow: $x_{\rm c} = 0.15R$. Green: $x_{\rm c} = 0.2R$. Blue: $x_{\rm c} = 0.25R$. Regions for lower values of $x_{\rm c}$ are not completely shown since they are covered by others. (C and D) x-dependence of the net dynein force on the CS, with dyneins located (C) on the cell boundary and (D) across the cortex. Black solid line: $x_{\rm c} = 0$. Red dashed line: $x_{\rm c} = 0.25R$. Green dotted line: $x_{\rm c} = 0.5R$. Blue dot-dashed line: $x_{\rm c} = 0.75R$. Purple dot-dot-dashed line: $x_{\rm c} = R$. (E) $x_{\rm c}$-dependence of the net dynein forces at $x = 0$. Solid circles: dyneins on cell boundary. Open circles: across the cortex. Forces are normalized by their maximum values at $x_{\rm c} = 0$.

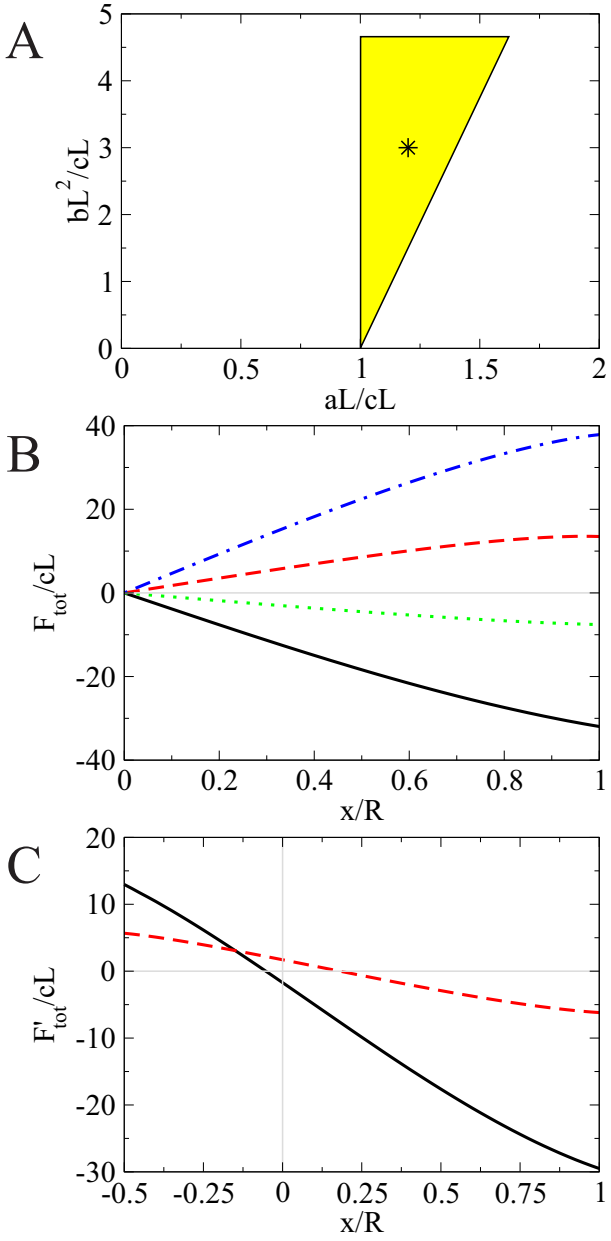

Figure S5. Results of the model with dynein and myosin mechanisms as above and alternative kinesin mechanism. (A) Region of suitable parameter values (yellow). The position of the chosen parameters $aL = 1.2cL$ and $bL^2 = 3cL$ is shown with the star. (B) x-dependence of the force on the CS. Solid black line: control cell. Dashed red line: dynein-inhibited cell. Dotted green line: myosin-inhibited cell. Blue dot-dashed line: cell with both dynein and myosin inhibited. (C) F-x relation for the nocodazole-affected cell (the nocodazole-affected wedge extends half-way to the center). Black solid line: control cell. Red dashed line: myosin-inhibited cell.

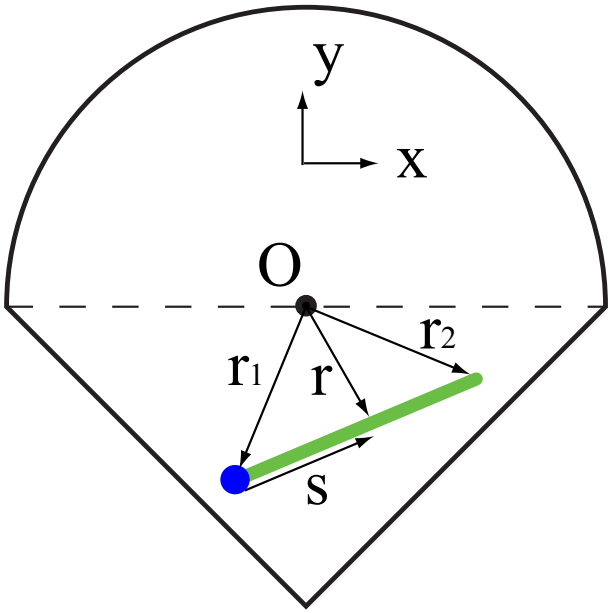

Figure S6. Schematic of force calculation in a fan-shaped cell.

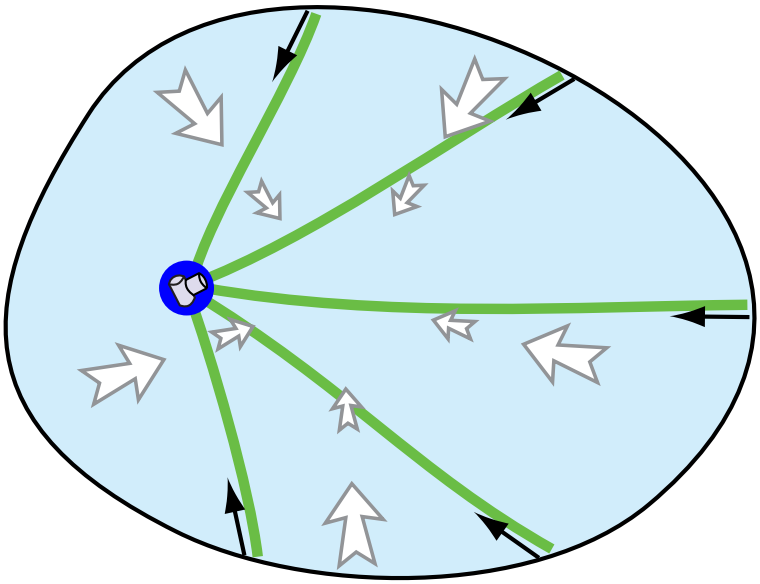

Figure S7. If the MT growth is biased to the distal cell edge when the CS shifts away from the center, then both MT pushing on the cell periphery and the actin centripetal flow mechanism destabilize the centering.